Chemical Engineering Journal 505 (2025) 159056

Contents lists available at ScienceDirect

Chemical Engineering Journal

journal homepage: www.elsevier.com/locate/cej

Accelerating direct formation of α-FAPbI$_3$ by dual-additives synergism for inverted perovskite solar cells with efficiency exceeding 26 %

Min Wang [1], Liang Li [1], Jinhui Wang, Hao Huang [*], Peng Cui, Zhineng Lan, Shujie Qu, Yi Suo, Meicheng Li [*]

State Key Laboratory of Alternate Electrical Power System with Renewable Energy Sources, School of New Energy, North China Electric Power University, Beijing 102206, China

ARTICLE INFO

Keywords:
Perovskite solar cells
α-FAPbI$_3$
Crystallization
Dual-additives
Phase purity

ABSTRACT

Improving the efficiency of inverted perovskite solar cells (PSCs) is crucial for promoting their commercialization. The α-FAPbI$_3$ shows huge promise as an absorber, however, its unfavored energetically at room temperature make the preparation of high-quality α-FAPbI$_3$ a challenge. In this work, the dual-additives were utilized to enhance the phase purity of α-FAPbI$_3$, and the underlined synergism was revealed. Both experimental measurement and theoretical calculation conformed that the dual-additives of MACl and PbCl$_2$ can synergistically enhance the ability to accelerate the direct formation of α-FAPbI$_3$ through largely reducing its formation energy, and inhibit the undesired δ-phase that inevitably occurs neither which additive is utilized singly. This synergism of dual-additives supports to realize a high-quality perovskite films with enhanced phase purity, and reduced defect density. As a consequence, the inverted PSCs achieve an impressive efficiency of 26.17 %, and the unencapsulated device can maintain 93 % of their initial PCE after 2000 h of storage in ambient air at 20 % RH and 25 ± 5 °C.

1. Introduction

Inverted perovskite solar cells (PSCs) possess remarkable advantages of competitive high PCE [1], long-term stability, and compatibility in tandem cells, making them promising in photovoltaic commercialization [2–4]. Attributing to the bandgap of 1.48 eV, the photoactive black phase α-FAPbI$_3$ is widely used as the absorber in high-efficiency inverted PSCs [5–7]. However, the formation of the α-FAPbI$_3$ is thermodynamically challenging, which makes it accompanied by other phases, normally δ-phase and solvent intermediate phase. The resultant films are prone to present multiscale imperfections, such as point defects, component heterogeneity, multiscale secondary, phases, and so on, resulting in less optimal optical bandgap, adverse optoelectronic properties [8–10]. Hence, revealing the crystallization kinetics of FAPbI$_3$ to gain an in-depth understanding of crystallization and effective regulation is necessary for the realization of high-efficiency PSCs.

The preparation of high-quality α-FAPbI$_3$ is the basis for obtaining efficient PSCs, and the solution process, such as one-step spin coating and two-step spin coating, are mostly utilized [11–16]. In the process of inverted PSCs, the perovskite films are normally obtained by one-step spin coating, the method we focused on in this work [17–21]. During the solvent process of α-FAPbI$_3$, polytype formation and the presence of other intermediate non-photoactive phases can readily occur, making it difficult to obtain pure-phase perovskite film. Reducing the formation energy of α-FAPbI$_3$ can promote its formation, which can be achieved by solvent engineering and additives [22–24]. For example, Bu et al. [25,26] regulated the ratio of N, N-dimethylformamide (DMF), dimethyl sulfoxide (DMSO), or N-methylpyrrolidone (NMP) in the perovskite precursor solvent, forming the adducts of PbI$_2$ and solvent, reducing the phase transition barrier of α-phase FAPbI$_3$, and achieving complete inhibition of unwanted δ-phase perovskite. Gao et al. [27] introduced low-solubility, halogen-rich CsPb$_2$Br$_5$ crystals into the perovskite solution and the results show that the CsPb$_2$Br$_5$ nanocrystals can induce direct crystallization of α-phase perovskite. This direct formation of α-phase instead of δ-phase effectively improves the crystal quality and increases the phase purity. Among the additives, Methylamine hydrochloride (MACl) is the most used. In 2019, Kim et al. [28] reported that MACl successfully induced the intermediate to α-FAPbI$_3$ phase without

* Corresponding authors.
E-mail addresses: hhuang@ncepu.edu.cn (H. Huang), mcli@ncepu.edu.cn (M. Li).
[1] These authors contributed equally.

https://doi.org/10.1016/j.cej.2024.159056
Received 1 October 2024; Received in revised form 24 December 2024; Accepted 27 December 2024
Available online 6 January 2025

annealing by reducing the formation energy. At present, the MACl almost has become the based component of perovskite precursor. However, even the MACl is used, α-$FAPbI_3$ formation suffers from adverse intermediate phase, negatively affecting the photovoltaic property by presented defects, undesirable residues, multiscale secondary phases and so on. Based on this situation, the use of binary or even multi-component additives is a promising option for further optimization of perovskite films. In 2024, Ding et al. [23] found that the use of 1,3-bis(cyanomethyl)imidazolium chloride ([Bcmim]Cl) in collaboration with MACl could effectively inhibit the degradation of perovskite precursors, inhibit the aggregation of MACl, preparing a homogeneous and stable perovskite film with high crystal degree and fewer defects. Considering the necessity of crystal regulation of perovskite films and the wide use of MACl additive, it is meaningful and necessary to explore the synergism between additives, and their effects on crystallization to obtain high-quality perovskite films and corresponding efficient PSCs.

Herein, we use dual-additives to regulate the α-$FAPbI_3$ crystallization and investigate the underline synergism, leading to perovskite film with enhanced phase purity and the corresponding PSCs with impressive efficiency. MACl, one of the dual-additives, has been proven to reduce the formation energy of α-$FAPbI_3$ and promote its formation, the crystallization process is still accompanied by the generation of δ-phase. Based on this residual undesirable δ-phase, lead (II) chloride ($PbCl_2$), the other of the dual-additives, has been used to inhibit the residual δ-phase synergistically with MACl, while synergistically enhancing the positive effect of MACl on crystallization. The synergy of these two additives can promote the direct formation of α-$FAPbI_3$, leading to a high-quality perovskite film with enhanced phase purity, reduced defect density, and prolonged carrier lifetime. These property optimizations translate to inverted PSCs achieved an impressive efficiency of 26.17 % with an aperture area of 0.08 cm^2, and the unencapsulated efficient device can maintain 93 % of their initial PCE after 2000 h storage in ambient air at 20 % RH and 25 ± 5 °C.

2. Results and discussion

Synergism of dual-additives regulates perovskite crystallization

We employed a one-step spin-coating method to fabricate perovskite films within a glovebox [18,20]. To investigate the impact of various dopants on the crystallization of perovskite films, we initially characterized the crystallization properties of the films, including surface micro-morphology, grains, and surface roughness, employing scanning electron microscopy (SEM) and atomic force microscopy (AFM). Four experimental groups were established, the control perovskite film, the film with MACl, the film with $PbCl_2$, and the film with MACl&$PbCl_2$, respectively.

As shown in Fig. 1a–d, all the perovskite films show characteristics of compact, pinhole-free, and full courage. In detail, after the use of additives, the average grain size of perovskite films increased slightly, and the dual-additives perovskite films obtained larger grains with the biggest average grain size, showing the synergism effect of dual-additives on optimizing crystallization. The cross-sectional images of four perovskite films were also obtained, which confirms that the thickness of approximately 700 nm, and the additives show a negligible influence on the film thickness (Fig. 1e–h). Compared to the control film, single additive, neither MACl nor $PbCl_2$ shows a slight effect on the crystallization, which is consistent with the SEM images. Notably, this optimization effect of additives on crystallization can be a collaborative enhancement, realizing the one greater than the sums of its part, which can be evidenced by the monolithic grain structure penetrating to the substrate of perovskite film with MACl&$PbCl_2$. To quantify the surface differences of different films, AFM was used to further characterize the surface morphology. As shown in Fig. 1i–l, where the AFM images were consistent with the SEM images described above, all the films show characteristics of compact, pinhole-free, and full courage. In detail, the root mean square (RMS) values of control film, film with MACl, film with $PbCl_2$, and film with MACl&$PbCl_2$ are 17.24, 16.71, 17.02, and 14.82 nm, respectively. Notably, the surface roughness of perovskite film after surface treatment was also measured and the value decreased after incorporating additives (Fig. S1). This optimized perovskite crystallization can also be validated by the film photos shown in Fig. S2, in which the film with MACl&$PbCl_2$ shows a smooth surface with a color of shiny black. From the above analysis results, it can be seen that the introduction of additives can effectively increase grain size, reduce

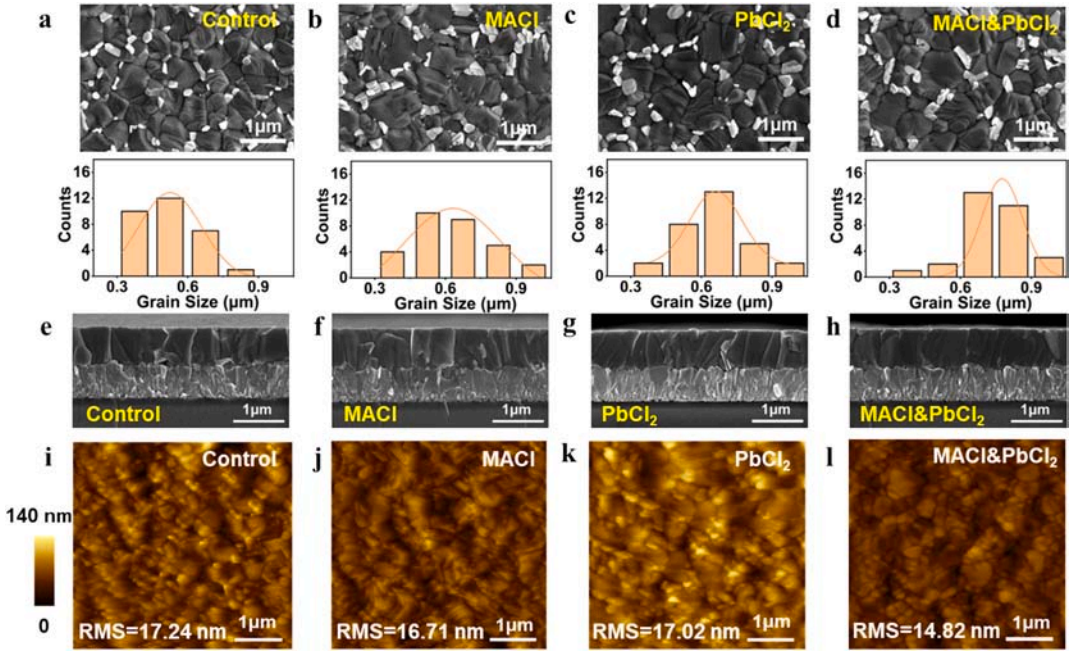

Fig. 1. Perovskite film morphology. (a-d) Top-view SEM images and grain size distribution of perovskite films without and with MACl, $PbCl_2$, MACl&$PbCl_2$ additive. (e-h) Cross-sectional SEM images of perovskite films without and with MACl, $PbCl_2$, MACl&$PbCl_2$ additive. (i-l) AFM images of perovskite films without and with MACl, $PbCl_2$, MACl&$PbCl_2$ additive.

surface roughness, and enhance the crystal orientation of perovskite, among which dual-additives have the best effect. The reduced surface roughness of the films is supposed to be conducive to the improvement of the layer-to-layer contact, which is expected to lead to a reduction in the series resistance at the interfaces [29–31].

To intuitively understand the effect of MACl, $PbCl_2$, and MACl&$PbCl_2$ additives on the crystallization kinetics of perovskites, we performed X-ray Diffraction (XRD) on perovskite films with different annealing times. As shown in Fig. 2a, as for the films without annealing, we can find that the MACl can promote the formation of α-$FAPbI_3$ and solvent phases comprising of $MA_2PbI_8Cl_{8-x}$·2DMSO. The $PbCl_2$ can also promote the formation of α-$FAPbI_3$. However, the $PbCl_2$ cannot induce the solvent phases, which differs from the effect of MACl. Although, both the MACl and $PbCl_2$ can effectively promote the formation of α-$FAPbI_3$, the film without annealing is still dominated by the δ-phase. Impressively, after introducing MACl&$PbCl_2$, the α-$FAPbI_3$ was apparently promoted and the δ-phase was inhibited, making the film dominated by the α-$FAPbI_3$. These results confirm that the synergism of dual-additives can collaboratively promote the formation of α-$FAPbI_3$ and inhibit the formation of δ-phase which is inevitable in film with single additive, thereby realizing the direct formation of α-$FAPbI_3$ and enhancing the phase purity at the initial state. Generally speaking, the formation of the α-$FAPbI_3$ is accompanied by other phases, normally δ-phase and solvent intermediate phase, in which the δ-phase is prone to possess more advantage in competition, which can be supported by the relatively lower formation energy of δ-phase than that of α-$FAPbI_3$ (Fig. 2c). The positive effect of additives can be well synergistic, leading to a much lower formation energy of α-$FAPbI_3$, further accelerating the direct formation of α-$FAPbI_3$ and companied solvent phase through circumventing the δ-phase. In short, we think that neither the single additive can be effective enough to make the formation of α-$FAPbI_3$ and solvent phase to obviously surpass the formation of δ-phase during the multi-phase competition, only the synergistic works of the dual-additives can eliminate the competitive advantage of δ-phase and induce the direct formation of α-$FAPbI_3$.

When annealing all films at different times, it is found that as the annealing time increased, the δ-phase perovskites in the control and the MACl, $PbCl_2$ films gradually convert into α phase perovskites. As for the film with MACl&$PbCl_2$, the directly formed α-$FAPbI_3$ keeps increasing and enhancing with the annealing processing, leading to a film with enhanced crystal orientation and crystallinity (Figs. S3-S5, Notes S1 and S2). The synergistic effect of dual-additives on promoting the direct formation of α-$FAPbI_3$ can also be validated by the photos of film placed at different times (Fig. 2b), where the wet film with MACl&$PbCl_2$ shows color of reddish-brown while other films are pale yellow. The color of the film with MACl&$PbCl_2$ can easily turn from reddish-brown to black in 10 s at room temperature, indicating the thermodynamically feasibility of $FAPbI_3$ crystallization. As a comparison, the control film cannot form the α-$FAPbI_3$ at room temperature, and the film with a single additive just shows a color of reddish-brown even after 420 s, indicating the partially formed α-$FAPbI_3$. To explain the directly formed α-$FAPbI_3$ by synergism of dual-additives, the density functional theory calculation was carried out to reveal the influence of different additives on the formation energy of α-$FAPbI_3$. As shown in Fig. 2c, both the additives of MACl and $PbCl_2$ possess the ability to reduce the formation energy of α-$FAPbI_3$, and this ability can be collaboratively enhanced, leading to the smallest formation energy of α-$FAPbI_3$ when using the dual-additives. This collaboratively decreased formation energy may explain the direct formation of α-$FAPbI_3$. We also monitored the direct formation of α-$FAPbI_3$ without annealing using in situ photoluminescent (PL) in a nitrogen glove box (Fig. 2d). In the initial phase, the precursor solution on the film takes on a sol–gel phase with a negligible PL signal

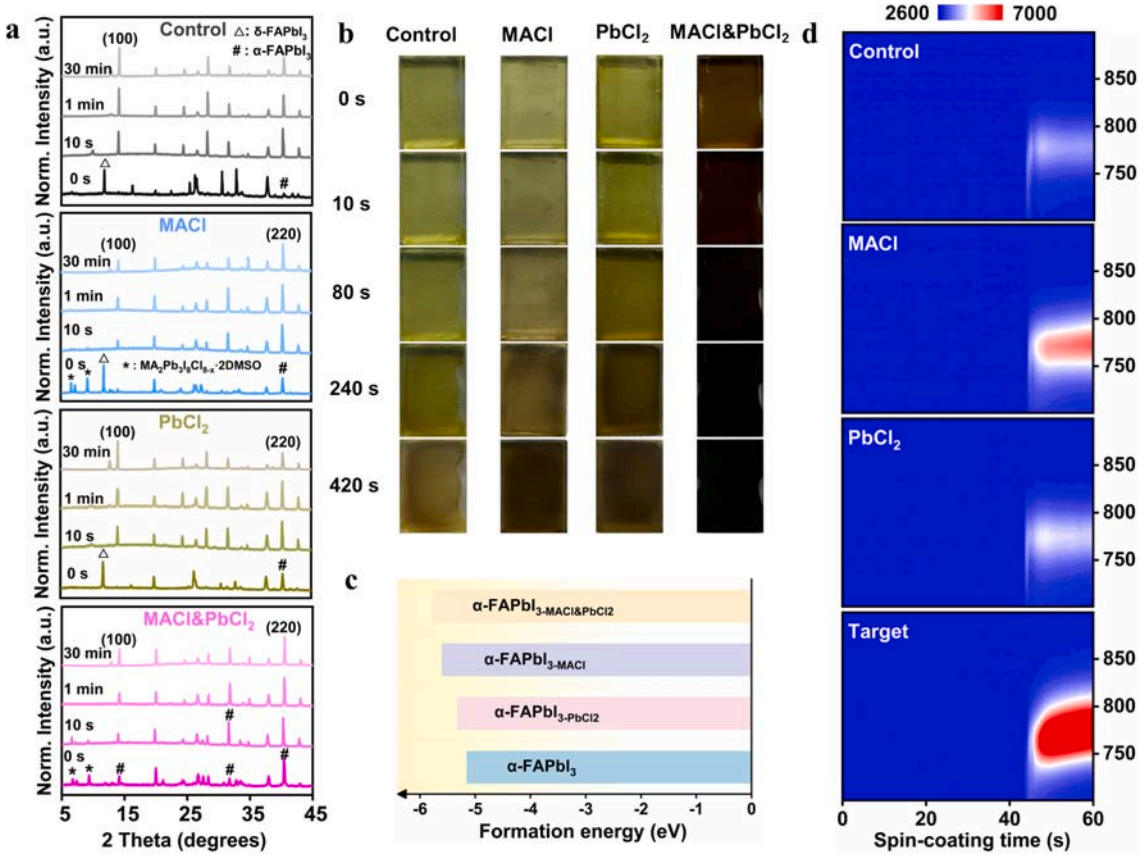

Fig. 2. Synergism revealing. (a) Perovskite thin film XRD annealed at different times. (b) color evolution over aging time at room temperature. (c) formation energy. (d) in situ PL spectra of the spin-coated perovskite films without and with MACl, $PbCl_2$, MACl&$PbCl_2$ additive.

in the range of 700–900 nm. When the anti-solvent is added to the rotating perovskite film at about 45 s, the PL emission intensity increases sharply within 5 s, indicating the rapid formation of $FAPbI_3$ nuclei in the film. MACl additives enhance the PL emission intensity of thin films more than $PbCl_2$ additives, and once both are used at the same time, the PL emission peak increases sharply. Among the films, the film with MACl&$PbCl_2$ shows the highest PL peak, confirming the direct formation of α-$FAPbI_3$, which is consistent with the results of XRD and film photos discussed above. Excepting from the peak intensity, we also notice the changes of the peak profiles, especially when using the dual-additives. Comparing to PL peaks of other samples, the peak of perovskite film with dual-additives shows wider range and obvious red shift, in which the wide range should result from the multiple perovskite phases with different composition, due to the dual-additives largely reduce the formation energy of perovskite and introduce excess MA^+, Cl^-, and the red shift should result from the transition from MA-based phase to FA-based phase due to the cation exchange [28,38,39].

3. Optical performance of perovskite films

The previous analysis results show that the introduction of additives can effectively improve the crystallization of perovskite films, in which MACl and $PbCl_2$ can synergistically accelerate the direct formation of α-$FAPbI_3$, leading to a perovskite film with larger grains and enhanced phase purity. After analyzing the effect of additive synergy on the crystallization of perovskite thin films, we further analyzed its impact on the optoelectronic properties of the films. Considering MACl additive is recognized as a common component of perovskite precursor, in the following discussion, we focus on discussing samples of perovskite with MACl and perovskite with MACl&$PbCl_2$, the latter is named as the target. We first carried out measurements of photoluminescence (PL) mapping, time-resolved photoluminescence (TRPL), PL, and electroluminescence (EL) on perovskite films. As depicted in Fig. 3a and b, the target perovskite film demonstrates a significantly enhanced fluorescence intensity in comparison to the film with MACl. In addition, the TRPL result (Fig. 3c and Table S1.) shows that the carrier lifetime of the target film is determined to be 1449.57 ns, more than four times longer than that (328.65 ns) of film with MACl. The PL and EL intensity of the target perovskite film is significantly higher than that of the perovskite film with MACl (Fig. S7 and S8). The Kelvin probe force microscopy (KPFM) measurement was also carried out to characterize the surface electrical property of the perovskite films (Fig. S9). Compared to perovskite film with MACl, the target film exhibits a lower average surface potential, which may be attributed to the decreased surface electronic tarp density. These results confirm that the dual-additives can effectively reduce the defects and it induced non-radiative recombination of perovskite film.

We also measured the optical properties of perovskite films using temperature-dependent PL emission. From Fig. 3d and e, it can be seen that the operating temperature has a significant impact on the PL luminescence of perovskite thin films. At a low temperature of 80 K, the film emits significant light due to the suppression of phonon emission. As the temperature increases, there is a marked reduction in the intensity of the PL peak. Furthermore, to delve deeper into the exciton dynamics within the perovskite material, the integrated intensity of the variable temperature photoluminescence (PL) peak was analyzed and fitted according to the Arrhenius equation [32]. of $I(T) = I_0/(1 + Ae^{-E_b/K_bT})$ (I_0 is the maximum signal, A is a constant, E_b is the thermal activation energy, K_b is the Boltzmann constant, and $I(T)$ is the photoluminescence intensity at 0 K). If no other nonradiative decay pathway exists in the recombination process, the thermal activation energy can be regarded as the exciton binding energy [33]. As shown in Fig. S10, after using dual-additives, the exciton binding energy of the perovskite film is 30.14 meV, while the perovskite film with MACl is 40.39 meV. This result further confirms that dual-additives are beneficial for charge separation and charge extraction in the device, which is beneficial to reducing carrier recombination [34,35]. In addition, we quantitively evaluated the defect density (N_t) of both types of films through the test of the space charge limited current of the electron-only device (F-doped tin oxide (FTO)/TiO_2/Perovskite/ETL/Ag) and hole-only device (FTO/

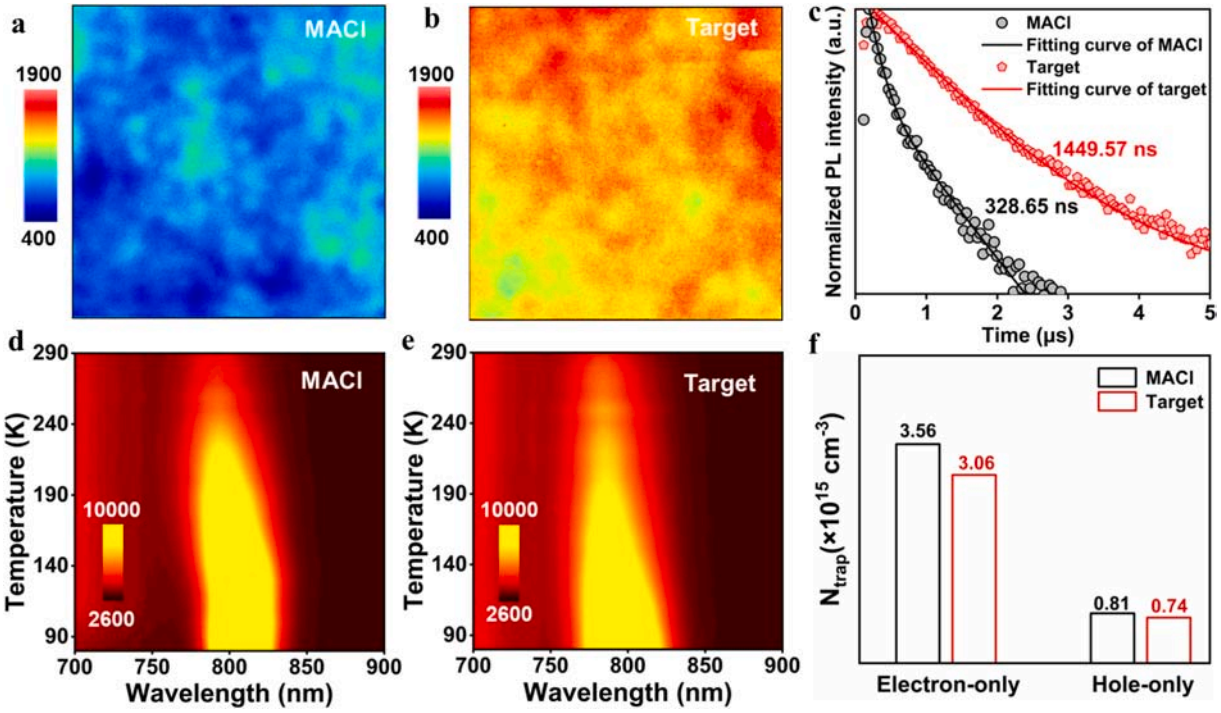

Fig. 3. Photoelectrical property of perovskite films. (a,b) PL mapping of MACl and target films. The detected size is 30 μm × 30 μm. (c) TRPL spectra of MACl and target films. (d, e) Temperature-dependent Photoluminescence of MACl and target films. (f) The defect density of MACl and target films was measured by using SCLC measurement.

HTL/Perovskite/2,2′,7,7′-tetrakis (*N*, *N*-dipmethoxyphenylamine)-9,9′spirobifluorene (Spiro-OMeTAD)/Ag) according to the equation of $N_t = 2\varepsilon_r\varepsilon_0 V_{TFL}/eL^2$ (ε_r is the relative permittivity, ε_0 the vacuum permittivity, e the electron charge, L the perovskite film thickness, and V_{TFL} the limiting voltage full of traps). As depict in Fig. 3f, after using dual-additives, the calculated N_t from the electron-only device decreased from 3.56×10^{15} cm^{-3} to 3.06×10^{15} cm^{-3}, the calculated N_t from the hole-only device decreased from 0.81×10^{15} cm^{-3} to 0.74×10^{15} cm^{-3}. The energy distribution of trap state density (tDOS) is used to visually measure the defect states in target PSCs and PSCs with MACl (Fig. S13). This result suggests that dual-additives can effectively reduce the density of deep trap states [40]. In addition, the influence of dual-additives on interfacial carrier dynamic was also explored using measurements of open circuit voltage decay (OCVD) and transient photocurrent (TPC) with both results indicate that the dual-additives show a positive effect on promoting interfacial carrier transport (Fig. S14). The reduction of defects in the perovskite film and promoted interfacial carrier transport help to inhibit non-radiation recombination, contributing to improving the photovoltaic performance of the PSCs [41,42].

4. Photovoltaic performance of PSCs

Based on the obtained high-quality perovskite film through synergism of dual-additives, we prepared inverted PSCs structured as FTO/nickel oxide (NiO_x)/[4-(3,6-Dimethyl-9*H*-carbazol-9-yl) butyl] phosphonic Acid (Me-4PACz)/perovskite/Fullerene (C_{60})/Bathocuproine (BCP)/Ag and investigated the effects of dual-additives on the photovoltaic performance. After determining the optimal concentration of additives (Figs. S15-S17, Note S3), the target PSCs achieved a champion PCE of 26.17 %, with short-circuit current density (J_{SC}) of 26.17 mA cm^{-2}, open-circuit voltage (V_{OC}) of 1.187 V, fill factor (FF) of 84.24 %, and the hysteresis is negligible (Fig. 4a and Fig. S18). As a comparison, the PSCs with MACl achieved a champion PCE of 24.91 %, with J_{SC} of 26.15 mA cm^{-2}, V_{OC} of 1.161 V, and FF of 82.06 %. The corresponding spectra of external quantum efficiency of target PSCs and PSCs with MACl are shown in Fig. 4b, and both the values of integrated J_{SC} show small variation with that in Fig. 4a. In addition, the stabilized power output of both PSCs was measured. The stabilized PCE of target PSCs is approximately 25.69 %, while the stabilized PCE of PSCs with MACl is approximately 24.62 % (Fig. S19).

To assess the reproducibility of the two types of PSCs, we collected photovoltaic parameters of 40 PSCs with MACl and target PSCs, respectively. The histogram of the PCE distribution showed that both PSCs exhibits good reproducibility. In detail, the target PSCs show an average PCE of 25.57 %, which is much higher than that (24.25 %) of PSCs with MACl (Fig. 4c). Fig. 4d shows the distribution of

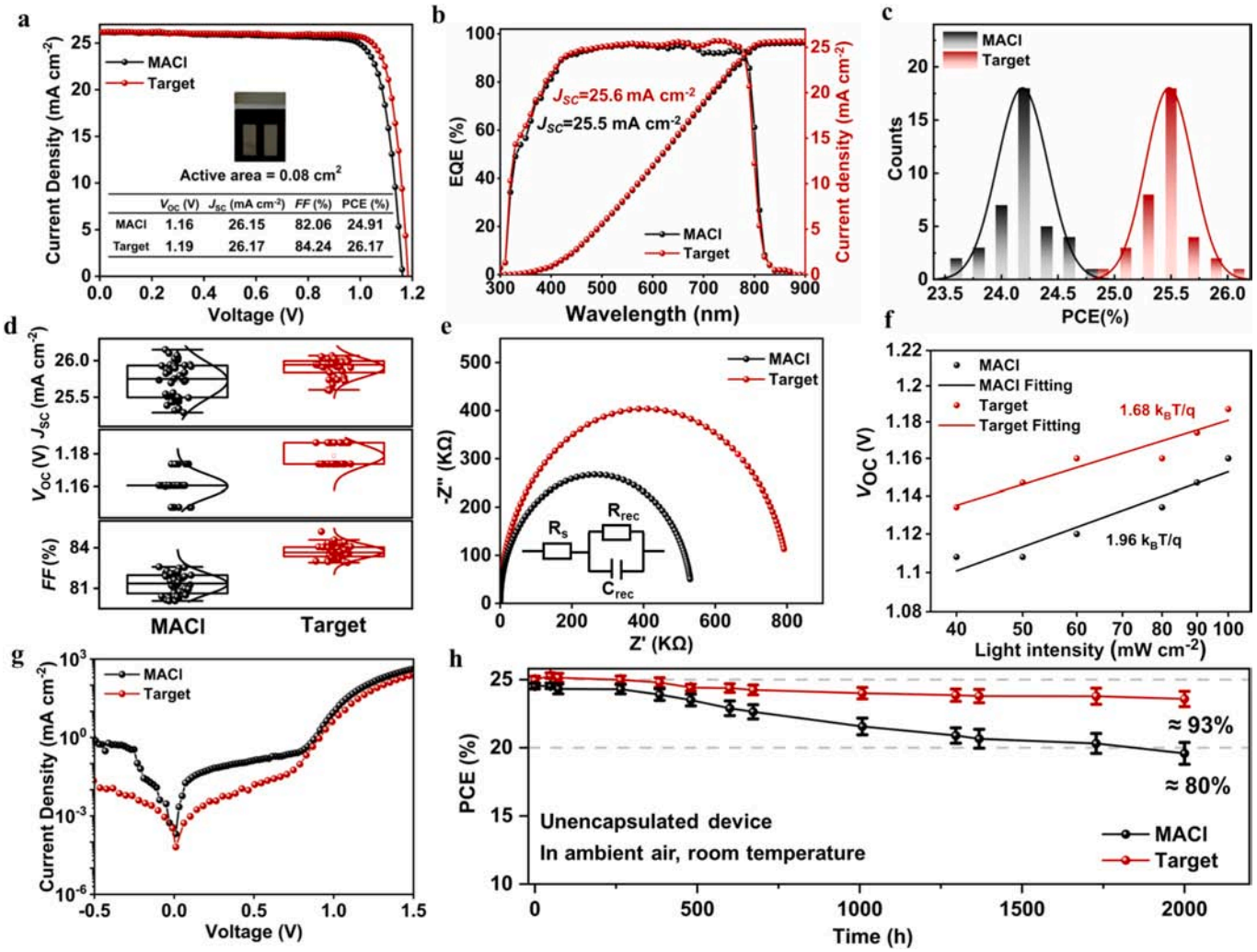

Fig. 4. Photovoltaic performance PSCs. (a) The reverse *J*–*V* curves of MACl and target PSCs with active area of 0.08 cm^2. (b) The EQE spectra of MACl and target PSCs. (c,d) Distribution histograms of PCE value and detailed photovoltaic parameters statistics among 40 PSCs. (e) EIS spectra of MACl and target PSCs. (f) The relationship between the V_{OC} of PSCs and light intensity. (g) Dark *J*–*V* curves of MACl and target PSCs. (h) PCE evolution of unencapsulated control and target PSCs stored under ambient air at 20 % RH and 25 ± 5 °C.

corresponding J_{SC}, V_{OC} and FF, where the target PSCs show an average J_{SC} of 25.90 mA cm^{-2}, average V_{OC} of 1.179 V, average FF of 83.74 %, and the PSCs with MACl only show an average J_{SC} of 25.73 mA cm^{-2}, average V_{OC} of 1.159 V, average FF of 81.33 %. From the detailed photovoltaic parameters, we can find that the increment of PCE mainly results from the increment of both V_{OC} and FF, which may be attributed to the suppressed non-radiative recombination that we are going to discuss in the following. We performed several measurements to investigate the physical properties of the device after using dual-additives, including the electrochemical impedance spectroscopy (EIS), dark *J–V* curves, and calculation of ideal factor (n_{ID}). Fig. 4e shows the EIS spectra of both PSCs, in which the target PSCs show a higher recombination resistance (8.08×10^5 ohm) than that (5.35×10^5 ohm) of PSCs with MACl, indicating the reduced recombination in target PSCs. In addition, the relationship between V_{OC} and light intensity was explored, further calculating the n_{ID} according to the equation of $V_{OC} = \frac{n_{ID}k_BT}{q} ln(I)$ (k_B is the Boltzmann constant and q represents the elementary charge). We calculated n_{ID} to be 1.96 and 1.68 for PSCs with MACl and target PSCs, respectively (Fig. 4f). The smaller n_{ID} indicates the reduced trap-assisted non-radiative recombination within the PSCs, and this reduced non-radiative recombination can also be validated by lower leakage current in the dark *J-V* curves (Fig. 4g) [36,37]. Based on the calculated ideal factor (n_{ID}), we further calculate the analytical maximum FF according to the following equation:

$$FF_{max} = \frac{\nu_{oc} - \ln(\nu_{oc} + 0.72)}{\nu_{oc} + 1} \; with \; \nu_{oc} = \frac{qV_{OC}}{n_{ID}k_BT}$$

Then, we added the S-Q FF value and experimental FF value to make a direct comparison to reveal that the increment of FF mainly results from the reduced non-radiative recombination loss (Fig. S20).

In addition to demonstrating the positive effect of the dual-additives on efficiency, we also explored its effect on the stability of PSCs. To evaluate the stability of PSCs under ambient conditions at 20 % RH and 25 ± 5 °C, we monitored the PCE evolution of unencapsulated PSCs after aging for 2000 h. As shown in Fig. 4h, target PSCs can maintain 93 % of their initial efficiency, while PSCs with MACl can only maintain 80 % of their initial efficiency after 2000 h. The operational stability was also investigated with the PSCs were continuously illuminated (white LED, 100 mW cm^{-2}) in the N_2-glovebox. The target PSCs can maintain 92 % of the original PCE after operating for 200 h, while the PSCs with MACl decline to 79 % of their initial value (Fig. S21). The enhanced device stability should be attributed to the optimized perovskite film with enhanced phase purity and reduced defect density.

5. Conclusion

In summary, we have achieved high-efficiency inverted PSCs through the synergism of dual-additives composed by the MACl and $PbCl_2$. The dual-additives of MACl and $PbCl_2$ are proven can synergistically enhance the ability to accelerate the direct formation of α-$FAPbI_3$ through largely reducing its formation energy, and inhibit the undesired δ-phase that inevitably occurs neither of which additive is utilized singly. Owing to the optimized perovskite film with enhanced phase purity, reduced defect density, and prolonged carrier lifetime, the resulting inverted PSCs achieved a PCE of 26.17 % with a high V_{OC} of 1.187 V, much higher than that (24.91 %) of PSCs only incorporating MACl. In addition, the device can maintain 93 % of the initial PCE after aging in ambient air for 2000 h, showing enhanced stability. We believe our approach of dual-additives and the revealed synergism provide a new idea for solving the bottleneck issues regarding the preparation of high-quality α-$FAPbI_3$ films, and more opportunities to achieve PSCs with excellent photovoltaic performance.

CRediT authorship contribution statement

Min Wang: Writing – original draft, Methodology, Investigation, Conceptualization. **Liang Li:** Writing – review & editing, Validation, Conceptualization. **Jinhui Wang:** Software, Investigation. **Hao Huang:** Writing – review & editing, Writing – original draft, Supervision. **Peng Cui:** Project administration, Methodology, Formal analysis. **Zhineng Lan:** Methodology, Formal analysis. **Shujie Qu:** Investigation, Formal analysis. **Yi Suo:** Validation, Investigation. **Meicheng Li:** Writing – review & editing, Supervision, Project administration, Conceptualization.

Declaration of competing interest

The authors declare that they have no known competing financial interests or personal relationships that could have appeared to influence the work reported in this paper.

Acknowledgments

This work is supported partially by the Key Research and Development Program sponsored by the Ministry of Science and Technology (MOST) (Grant nos. 2022YFB4200301), National Natural Science Foundation of China (Grant nos. 52232008, 51972110, 52102245, 52072121, 52402254, 22109002 and 22409061), Beijing Natural Science Foundation (2222076, 2222077, Z240024), Beijing Nova Program (20220484016), Young Elite Scientists Sponsorship Program by CAST (2022QNRC001), 2022 Strategic Research Key Project of Science and Technology Commission of the Ministry of Education, Huaneng Group Headquarters Science and Technology Project (HNKJ20-H88), State Key Laboratory of Alternate Electrical Power System with Renewable Energy Sources (LAPS2024-05), the Fundamental Research Funds for the Central Universities (2022MS029, 2022MS02, 2022MS031, 2023MS042, 2023MS047, 2023MS042, 2023MS047) and the NCEPU “Double First-Class” Program.

Appendix A. Supplementary data

Supplementary data to this article can be found online at https://doi.org/10.1016/j.cej.2024.159056.

Data availability

Data will be made available on request.

References

[1] Chart (2024). https://www.nrel.gov/pv/cell-efficiency.html/.
[2] A. Al-Ashouri, E. Köhnen, B. Li, A. Magomedov, H. Hempel, P. Caprioglio, J. A. Márquez, A.B. Morales Vilches, E. Kasparavicius, J.A. Smith, Monolithic perovskite/silicon tandem solar cell with> 29% efficiency by enhanced hole extraction, Science 370 (2020) 1300–1309.
[3] R. Lin, J. Xu, M. Wei, Y. Wang, Z. Qin, Z. Liu, J. Wu, K. Xiao, B. Chen, S.M. Park, All-perovskite tandem solar cells with improved grain surface passivation, Nature 603 (2022) 73–78.
[4] Y.-H. Lin, N. Sakai, P. Da, J. Wu, H.C. Sansom, A.J. Ramadan, S. Mahesh, J. Liu, R. D. Oliver, J. Lim, A piperidinium salt stabilizes efficient metal-halide perovskite solar cells, Science 369 (2020) 96–102.
[5] J.W. Lee, D.J. Seol, A.N. Cho, N.G. Park, High-efficiency perovskite solar cells based on the black polymorph of $HC(NH_2)_2PbI_3$, Adv. Mater. 26 (2014) 4991–4998.
[6] T.M. Koh, K. Fu, Y. Fang, S. Chen, T.C. Sum, N. Mathews, S.G. Mhaisalkar, P. P. Boix, T. Baikie, Formamidinium-containing metal-halide: an alternative material for near-IR absorption perovskite solar cells, J. Phys. Chem. C 118 (2014) 16458–16462.
[7] E. Smecca, Y. Numata, I. Deretzis, G. Pellegrino, S. Boninelli, T. Miyasaka, A. La Magna, A. Alberti, Stability of solution-processed $MAPbI_3$ and $FAPbI_3$ layers, PCCP 18 (2016) 13413–13422.
[8] W. Hui, L. Chao, H. Lu, F. Xia, W.J.S. Huang, Stabilizing black-phase formamidinium perovskite formation at room temperature and high humidity, Science 371 (6536) (2021) 1359–1364.

[9] T. Chen, J. Xie, B. Wen, Q. Yin, R. Lin, S. Zhu, P.J.N.C. Gao, Inhibition of defect-induced α-to-δ phase transition for efficient and stable formamidinium perovskite solar cells, Nat. Commun. 14 (1) (2023) 6125.
[10] P. Shi, Y. Ding, B. Ding, Q. Xing, T. Kodalle, C.M. Sutter-Fella, R. Wang, Oriented nucleation in formamidinium perovskite for photovoltaics, Nature 620 (2023) 323–327.
[11] L. Yan, H. Huang, P. Cui, S. Du, Z. Lan, Y. Yang, S. Qu, X. Wang, Q. Zhang, B. Liu, Fabrication of perovskite solar cells in ambient air by blocking perovskite hydration with guanabenz acetate salt, Nat. Energy 8 (2023) 1158–1167.
[12] S. Du, H. Huang, Z. Lan, P. Cui, L. Li, M. Wang, S. Qu, L. Yan, C. Sun, Y. Yang, Inhibiting perovskite decomposition by a creeper-inspired strategy enables efficient and stable perovskite solar cells, Nat. Commun. 15 (2024) 5223.
[13] X. Wang, H. Huang, M. Wang, Z. Lan, P. Cui, S. Du, Y. Yang, L. Yan, Q. Zhang, S. Qu, Oriented molecular bridge constructs homogeneous buried interface for perovskite solar cells with efficiency over 25.3%, Adv. Mater. 36 (2024) 2310710.
[14] Z. Lan, H. Huang, Y. Lu, S. Qu, M. Wang, S. Du, Y. Yang, C. Sun, Q. Zhang, Y. Suo, Homogenizing the electron extraction via eliminating low-conductive contacts enables efficient perovskite solar cells with reduced up-scaling losses, Adv. Funct. Mater. (2024) 2316591.
[15] H. Huang, P. Cui, Y. Chen, L. Yan, X. Yue, S. Qu, X. Wang, S. Du, B. Liu, Q. Zhang, 24.8%-efficient planar perovskite solar cells via ligand-engineered TiO_2 deposition, Joule 6 (2022) 2186–2202.
[16] X. Zhao, Y. Qiu, M. Wang, D. Wu, X. Yue, H. Yan, B. Fan, S. Du, Y. Yang, Y. Yang, Regulation of buried interface through the rapid removal of PbI_2·DMSO complex for enhancing light stability of perovskite solar cells, ACS Energy Lett. 9 (2024) 2659–2669.
[17] S. Liu, J. Li, W. Xiao, R. Chen, Z. Sun, Y. Zhang, X. Lei, S. Hu, M. Kober-Czerny, J. Wang, Buried interface molecular hybrid for inverted perovskite solar cells, Nature (2024) 1–3.
[18] Z. Li, X. Sun, X. Zheng, B. Li, D. Gao, S. Zhang, X. Wu, S. Li, J. Gong, J.M. Luther, Stabilized hole-selective layer for high-performance inverted pin perovskite solar cells, Science 382 (2023) 284–289.
[19] S. Yu, Z. Xiong, H. Zhou, Q. Zhang, Z. Wang, F. Ma, Z. Qu, Y. Zhao, X. Chu, X. Zhang, Homogenized NiO_x nanoparticles for improved hole transport in inverted perovskite solar cells, Science 382 (2023) 1399–1404.
[20] Q. Tan, Z. Li, G. Luo, X. Zhang, B. Che, G. Chen, H. Gao, D. He, G. Ma, J. Wang, Inverted perovskite solar cells using dimethylacridine-based dopants, Nature 620 (2023) 545–551.
[21] H. Tang, Z. Shen, Y. Shen, G. Yan, Y. Wang, Q. Han, L.J.S. Han, Reinforcing self-assembly of hole transport molecules for stable inverted perovskite solar cells, Science 383 (2024) 1236–1240.
[22] W. Hui, L. Chao, H. Lu, F. Xia, W. Huang, Stabilizing black-phase formamidinium perovskite formation at room temperature and high humidity, Science 371 (2021) 1359–1364.
[23] B. Ding, Y. Ding, J. Peng, J. Romano-deGea, L.E. Frederiksen, H. Kanda, O. A. Syzgantseva, M.A. Syzgantseva, J.-N. Audinot, J. Bour, Dopant-additive synergism enhances perovskite solar modules, Nature 628 (2024) 299–305.
[24] Y. Chen, N. Yang, G. Zheng, F. Pei, W. Zhou, Y. Zhang, L. Li, Z. Huang, G. Liu, R. Yin, Nuclei engineering for even halide distribution in stable perovskite/silicon tandem solar cells, Science 385 (2024) 554–560.
[25] T. Bu, J. Li, H. Li, C. Tian, F.J.S. Huang, Lead halide-templated crystallization of methylamine-free perovskite for efficient photovoltaic modules, Science 372 (2021) 1327–1332.
[26] Z.X. A, L.Z. B, J.H. A, Z.W. A, P.Z. C, C.J.B.D. E, K.F. E, Y.M. A, F.G.A. F, Reducing energy barrier of δ-to-α phase transition for printed formamidinium lead iodide photovoltaic devices, Nano Energy 91 (2022) 106658.
[27] C. Gao, K. Gao, B.J.E. Zhang, e.s. EES, $CsPb_2Br_5$-assisted direct crystallization of the 3D perovskite phase for highly efficient and stable solar cells, 17 (2024) 2734-2742.
[28] M. Kim, G.-H. Kim, T.K. Lee, I.W. Choi, H.W. Choi, Y. Jo, Y.J. Yoon, J.W. Kim, J. Lee, D. Huh, H. Lee, S.K. Kwak, J.Y. Kim, D.S. Kim, Methylammonium chloride induces intermediate phase stabilization for efficient perovskite solar cells, Joule 3 (2019) 2179–2192.
[29] P. Shi, J. Xu, I. Yavuz, T. Huang, S. Tan, K. Zhao, X. Zhang, Y. Tian, S. Wang, W. Fan, Strain regulates the photovoltaic performance of thick-film perovskites, Nat. Commun. 15 (2024) 2579.
[30] H. Zhang, W. Xiang, X. Zuo, X. Gu, S. Zhang, Y. Du, Z. Wang, Y. Liu, H. Wu, P. Wang, Fluorine-containing passivation layer via surface chelation for inorganic perovskite solar cells, Angew. Chem. 135 (2023) e202216634.
[31] T. Nie, Z. Fang, T. Yang, K. Zhao, J. Ding, S. Liu, Anti-Solven-Free preparation for efficient and photostable pure-iodide wide-bandgap perovskite solar cells, Angew. Chem. Int. Ed. 63 (2024) e202400205.
[32] B. Jin, N. Zuo, Z. Hu, W. Cui, R. Wang, G.V. Tendeloo, X. Zhou, T. Zhai, Excellent excitonic photovoltaic effect in 2D $CsPbBr_3$/CdS heterostructures, Adv. Funct. Mater. 30 (2020) 2006166.
[33] Z. Yang, M. Wang, H. Qiu, X. Yao, X. Lao, S. Xu, Z. Lin, L. Sun, J.J.A.F.M. Shao, Engineering the exciton dissociation in quantum-confined 2D $CsPbBr_3$ nanosheet films, Adv. Funct. Mater. 28 (2018) 1705908.
[34] F. Ruf, M.F. Aygüler, N. Giesbrecht, B. Rendenbach, A. Magin, P. Docampo, H. Kalt, M.J.A.M. Hetterich, Temperature-dependent studies of exciton binding energy and phase-transition suppression in (Cs, FA, MA)Pb(I, Br)$_3$ perovskites, APL Mater. 7 (2019).
[35] N. Li, X. Niu, L. Li, H. Wang, H.J.S. Zhou, Liquid medium annealing for fabricating durable perovskite solar cells with improved reproducibility, Science 373 (2021) 561–567.
[36] Y. Yang, H. Huang, L. Yan, P. Cui, Z. Lan, C. Sun, S. Du, X. Wang, C. Yao, S.J.A.E. M. Qu, Compatible soft-templated deposition and surface molecular bridge construction of SnO_2 enable air-fabricated perovskite solar cells with efficiency exceeding 25.7%, Adv. Energy Mater. (2024) 2400416.
[37] L. Yang, J. Feng, Z. Liu, Y. Duan, S. Zhan, S. Yang, K. He, Y. Li, Y. Zhou, N.J.A. M. Yuan, Record-efficiency flexible perovskite solar cells enabled by multifunctional organic ions interface passivation, Adv. Mater. 34 (2022) 2201681.
[38] L. Chen, M. Hu, S. Lee, J. Kim, Z.Y. Zhao, S.P. Han, S.I. Seok, Deciphering reaction products in formamidine-based perovskites with methylammonium chloride additive, J. Am. Chem. Soc. 145 (2023) 27900–27910.
[39] J. Hu, J.W. Ahn, Z. Xu, M.J. Jeong, C. Kim, J.H. Noh, B.P. Rand, Iodine modulates the MACl-assisted growth of $FAPbI_3$ for high efficiency perovskite solar cells, Adv. Energy Mater. (2024) 2400500.
[40] J. Hong, Z. Xing, D. Li, B. Hu, K. Xu, X. Hu, Y. Chen, Managing solvent complexes to amplify ripening process by covalent interaction driving force under external field for perovskite photovoltaic, Adv. Mater. (2024) 2409971.
[41] Y. Zhang, L. Xu, J. Sun, Y. Wu, Z. Kan, H. Zhang, H. Song, 24.11% high performance perovskite solar cells by dual interfacial carrier mobility enhancement and charge-carrier transport balance, Adv. Energy Mater. 12 (2022) 2201269.
[42] S. Wang, L. Tan, J. Zhou, M. Li, X. Zhao, H. Li, C. Yi, Over 24% efficient MA-free $Cs_xFA_{1-x}PbX_3$ perovskite solar cells, Joule 6 (2022) 1344–1356.